Study on Combustion Performance of the Radial Staged Combustion Chamber with Lobed Nozzles

*WANG Lijun**, *FAN Jingpeng*, *MEN Kuo*, *XU Yijun*

College of Energy and Environment, Shenyang Aerospace University, Shenyang 110136, P. R. China

(Received 9 March 2022; revised 15 July 2022; accepted 2 August 2022)

Abstract: In order to investigate the effect of the radial gradation of the lobed nozzles on the flow field organization, a cold water model experimental platform for a combustion chamber with radial-staged 13-point lobed nozzles is built. Compared with a series of combustion OH* luminescence experiments tested by the University of Cincinnati, the four corresponding working conditions of no load, partial load, cruise and take off are selected. The vortex structure, vorticity value, multi-combustion materiel field and combustion characteristics of the flow field in the radial staged combustion chamber of the lobed nozzles under the equivalence ratio, the fuel injection method, the fuel injection ratio and other factors are numerically studied. The results show that under different influencing factors, the varation trend of the hydroxyl flame field of the lobe combustion chamber is basically the same as that of the hydroxyl light emission experiment of the swirl combustion chamber, but the flame field shape is quite different. The local equivalent ratio has a greater influence on the relevant combustion performance of the combustion chamber. Under the conditions of lower equivalence ratio, three-stage air and fuel injection mode, and gradually transferring the fuel flow of the pilot circuit to the external circuit, the temperature field and flame field of the combustion chamber are more evenly distributed, the outlet temperature field quality is better, the combustion efficiency is higher, and the NO_X emission is relatively low. These are basically consistent with the cold test results. The cold experimental results illustrate the importance of the influence of the flow field organization on the combustion organization and verify the reliability of the calculation results.

Key words: lobed nozzle; radial-staged combustion; aerodynamic characteristic; combustion characteristic

CLC number: V231.3 **Document code:** A **Article ID:** 1005-1120(2022)05-0619-18

0 Introduction

Modern aero-engine combustion chambers are increasingly designed to have a lean local equivalence ratio with high levels of mixing to reduce temperature peaks[1]. The fuel injection method can affect the organization of oil and gas in the combustion chamber. It has a great influence on the local equivalence ratio in the combustion chamber, therefore, it has a decisive influence on the combustion organization of the combustion chamber.

In response to the needs of modern aeroengines, the lean direct injector (LDI) combustor has been proven to be a lean burn combustor in a promising future[2]. The so-called "direct" injection of fuel into the combustion zone means that when the temperature and pressure at the inlet of the combustion chamber increase, and the fuel burns during the mixing process, the ignition delay time will be greatly shortened. When multiple small-sized fuel nozzles are used instead of the traditional large-sized nozzles, the transportation distance will be reduced, the mixing speed will be accelerated, the uniformity of the fuel and air mixture will be improved, and the local hot spots will be reduced[3]. The overall average flame temperature in the combustion chamber can be kept at a low level. The LDI concept was originally

*Corresponding author, E-mail address: wanglijun@sau.edu.cn.

How to cite this article: WANG Lijun, FAN Jingpeng, MEN Kuo, et al. Study on combustion performance of the radial-staged combustion chamber with lobed nozzles[J]. Transactions of Nanjing University of Aeronautics and Astronautics, 2022, 39(5): 619-636.

http://dx.doi.org/10.16356/j.1005-1120.2022.05.010

designed to meet the emissions requirements of International Civil Aviation Organization (ICAO) that NO_X emissions should be halved by 2026[4]. It mainly relies on controlling the blending combustion of oil and gas in the lean combustion zone and reducing the flame temperature and NO_X emissions.

The fuel staging concept is to control the load by dividing the fuel supply into different fuel circuits. Only one fuel circuit is required in the no-load state, 2—3 fuel circuits in the cruise state, and 3 fuel circuits in the take-off state[5]. In the past, few studies have been done on the multi-nozzle array LDI combustion chamber. In recent years, scholars have paid more attention to the multi-point fuel nozzle flexible injection combustion chamber[6-7]. Based on the work of University of Cincinnati, National Aeronautics and Space Administration(NASA) has conducted an extensive research on the LDI staged combustion system. They carried out a systematic study on the 13-point nozzles grading arrangement, and its focus was on the grading combustor technology, with the goal of reducing NO_X emissions during landing and takeoff cycles[8]. Compared with the traditional single large-size nozzle injection method, the NO_X content of combustion in the staged injection method is much lower[9]. At present, under the staged combustion mode, the focus is the NO_X emission of the combustion chamber. However, there are few studies about the influence of the flow field organization of the staged combustion chamber on the combustion organization, as well as the performance parameters such as outlet temperature distribution coefficient, combustion efficiency and total pressure loss. The research shows that under different inlet conditions, the fuel staged injection has a great influence on the droplet size, shape and flame structure of the fuel spray in the reaction zone[10]; and the temperature will increase with the increase of the equivalence ratio.

The number and arrangement of different nozzles in the LDI staged combustion system have a large impact on the combustion field. Tacina et al.[11-12] conducted a series of early operable partial and overall emission tests on the multipoint lean direct injector (MLDI) sector and 9-point and 25-point uniform array arrangements. Studies have shown that under a high-load operation and a high oil-gas ratio, the MLDI system outputs low NO_X emissions and good flame stability as the number of nozzles increases. However, with the number of nozzles increasing for low load conditions, the fuel injection volume of a single nozzle becomes quite low, and effective fuel injection cannot be achieved[13]. A 9-nozzle array fuel planner laser induced fluorescence(PLIF) image measured by Hicks et al.[14] showed that using multiple injection positions can quickly and efficiently atomize fuel. Moreover, the use of segmented and alternating nozzles can significantly reduce the distribution factor of turbine inlet temperature.

Different fuel injection methods and distribution ratios have a large impact on the flame position and spatial temperature distribution in the combustion chamber[15]. In view of the previous research results, the lobed nozzle array in this paper adopts a 13 points 5×5 alternate arrangement of fork rows. Compared with the hydroxy light emission experiment of the multi-point spin-flow nozzle combustion chamber, we conduct an in-depth study on the flame position and distribution of the combustion chamber with radial stayed lobed nozzles under different operating conditions. The lobed nozzles are originally used to study mixing process between primary and secondary flows. In recent years, Li et al.[16-17] have used lobe hydrocyclones instead of blade hydrocyclones to improve fuel/air mixing process and flame stability. Based on the study of NO_X emissions from different loads, the combustion efficiency, outlet temperature distribution coefficient, total pressure loss and other combustion characteristics of the targeted combustion chamber under different influencing factors have been studied.

1 System Description

1.1 Calculation model

The radial staged combustor system studied in this paper was developed by the United Technologies Aerospace System (UTAS), and the lobed nozzles are used to replace the spin flow nozzles. The entire system (Fig.1(a)) consists of an inverted cone combustion chamber body and a multi-point lobed nozzle array. Multi-point means that the tradi-

tional single large nozzle is replaced by multiple small nozzles. The combustion chamber system is composed of 13 small nozzle arrays that are arranged in an alternating arrangement of 5×5 fork rows (Fig.1(b)). The horizontal and vertical distances between the edge of the lobe are 14 mm, and the distance from the edge of the outer lobe to the edge of the combustion chamber is 15.9 mm. The lobed nozzle (Fig.1(c)) adopts a 6-petal structure[18]. The entrance diameter is 15 mm. The entrance parallel end length is 15 mm. The lobe length is 10 mm. The lobe diameter is 24 mm. The inner ring diameter is 8 mm. And the peak and trough diameters are 3.5 mm. The total length of the combustion chamber is 255.8 mm. The side length of the front end is 207.8 mm. The side length of the trailing end is 83 mm. And the length of the parallel exit is 40 mm.

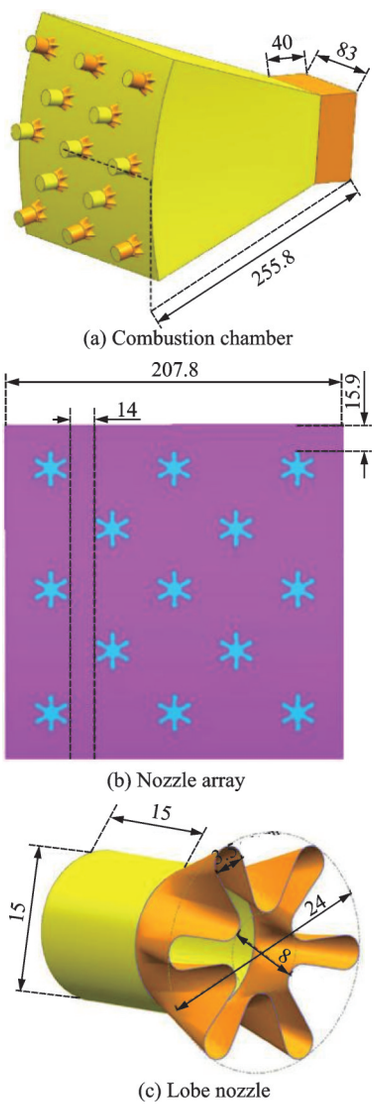

Fig.1 Geometric model of combustion chamber

1.2 Grid independence verification

Integrated computer engineering and manufacturing code for computational fluid dynamics(ICEM-CFD) meshing of ANSYS software is performed on the calculation model. Since the peaks and troughs of the lobed nozzle vary are great, this paper uses an unstructured grid for the entire calculation model. The lobed nozzle uses five layers of boundary layer encryption. Case-6 (Take off) grid independence test results (Table 1) show that the average exit speed and average temperature obtained by the three different numbers of grids are relatively close, and the difference between the number of the last two adjacent grids is small. The helicity in Fig.2 represents the vorticity values where the X axis represents various positions in the flow direction of the combustion chamber. It can also be seen from Fig.2 that the difference in the vorticity values of the latter two flow vortices at various positions in the flow direction of the combustion chamber is small. Taking into account the calculation results, calculation accuracy and calculation time, the total number of meshes ultimately used is about 2.96 million.

Table 1 Grid independence verification results

Number of grids/ 10^6	Average outlet speed/(m·s^{-1})	Average outlet temperature/K
2.61	2.72	1 279.8
2.96	2.58	1 305.6
3.22	2.53	1 313.5

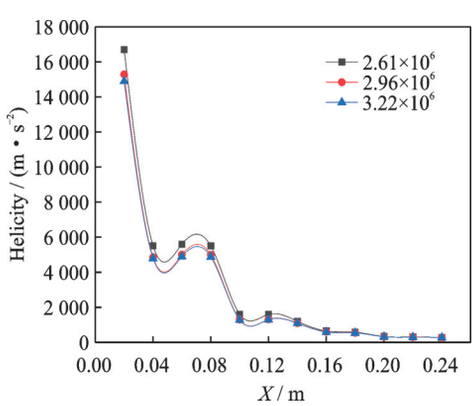

Fig.2 Grid independence verification results

1.3 Physical model and schem

The selection of turbulence model mainly considers the problems involved in the flow process and the amount of computer resources occupied. Xie et al.[19] used different turbulence models to explore

the applicability of lobed nozzles. For the calculation process of the aero-engine combustion chamber, considering the above two factors and the test results, we select the two equation k-e models. Among them, the realizable k-e model has a good effect in the calculation of nozzle jet mixing and other problems, so the realizable k-e turbulence model is selected in the calculation process. The pressure gradient of the flowing inside the aeroengine combustion chamber is small, and the turbulent dissipation does not change much at the wall surface. The wall surface adopts the standard wall function method. The aero-engine combustion process is a two-phase flow, and the discrete phase model uses the Euler-Lagrange method. The fuel spray model uses the conical nozzle model. The combustion process in aero-engines is mainly turbulent diffusion flame, so the non-premixed combustion model is used for combustion model. The Euler-Lagrange random walk model is adopted for fuel particles, and the particle sizes follow the Rosin-Rammler distribution. The beta probability density function is adopted to describe the kerosene particles distribution. The equilibrium chemical model is used for chemical reaction mechanisms. Eleven components are considered in the combustion calculation, including $C_{12}H_{23}$, CH_4, CO, CO_2, H_2, H_2O, O_2, H, OH, N_2, and C(s). The multi-step simplification reaction mechanism is used for combustion process, and the discrete ordinates (DO) radiation model is adopted to calculate the radiative heat transfer .

The boundary condition inlet is based on the mass inlet. We select the pressure outlet and the mixed wall surface for our study. We also use the SIMPLEC algorithm. We adopt the cell based green-Gauss for the variable gradient in the difference format, the standard format for the pressure term, and the second-order upwind style for the kinetic energy term and the turbulence term. The equation convergence accuracy setting converges to 10^{-5}. Since the combustion chamber studied in this paper contains multiple inlets, the hybrid initialization method is used.

The five rows of the radial lobed nozzles in the system are designed as three fuel circuits. They can be opened and closed as required, and the fuel flow of each fuel circuit can be controlled individually. The air distribution ratio of different types of fuel nozzles is as follows: The center pilot row nozzles provide 12.4% of the air to the combustion chamber; the middle two rows of nozzles provide 38.8%; and the outermost two rows provide 48.8%. The three fuel circuits can flexibly change the fuel distribution ratio. All the five rows of nozzles are for high power refueling such as take-off and landing. The center pilot row and the middle row nozzles are for partial load refueling. And the center pilot row nozzles are only for no-load refueling. This method of fuel grading is to provide full operability from idle to take-off, cruise and landing. For the convenience of the following discussion, only the center pilot row nozzle fuel injection is marked as "P"; the center pilot row and the intermediate two rows of fuel are marked as "PI", and all the five rows of fuel are marked as "PIO". The parameter "FS" is used to describe the fuel distribution and represents the ratio of fuel flow through a fuel circuit to the total flow. For example, "FS_{pilot}" represents the center pilot exhaust circuit fuel flow rate / total fuel flow rate. The specific calculation and simulation conditions are shown in Tables 2—6.

Table 2 Calculation conditions of unload (only pilot with varying ϕ)

Condition	ϕ	ϕ_P	T_3/K	p_4/kPa	Δ_P/%
Case 1	0.19	1.53	496	100	4.1
Case 2	0.25	2.02	496	100	4.1
Case 3	0.36	2.90	496	100	4.1
Case 4	0.40	3.23	496	100	4.1

Table 3 Calculation conditions of partial load (pilot and intermediate fuel circuits with varying ϕ and fuel split)

Condition	FS_{pilot}	ϕ	ϕ_P	ϕ_I	T_3/K	p_4/kPa	Δ_P/%
Case 1	0.35	0.35	1.01	0.59	496	360	4
Case 2	0.35	0.41	1.18	0.68	496	360	4
Case 3	0.27	0.35	0.78	0.67	496	360	4
Case 4	0.25	0.41	0.82	0.79	496	360	4

Table 4 Calculation conditions of cruise (pilot and intermediate fuel circuits with varying fuel split)

Condition	FS_{pilot}	ϕ	ϕ_P	ϕ_I	T_3/K	p_4/kPa	Δ_P/%
Case 1	0.60	0.41	2.00	0.42	496	360	4
Case 2	0.50	0.41	1.67	0.53	496	360	4
Case 3	0.36	0.41	1.18	0.68	496	360	4
Case 4	0.25	0.41	0.82	0.79	496	360	4

Table 5 Calculation conditions of cruise

Condition	FS_{pilot}	$FS_{intermediate}$	FS_{outer}	ϕ	ϕ_P	ϕ_I	ϕ_O	T_3/K	p_4/kPa	Δ_P/%
Case 1	0.26	0.32	0.42	0.41	0.86	0.34	0.35	496	360	4
Case 2	0.19	0.36	0.45	0.41	0.63	0.38	0.38	496	360	4
Case 3	0.16	0.37	0.47	0.41	0.53	0.39	0.40	496	360	4
Case 4	0.12	0.39	0.49	0.41	0.40	0.41	0.41	496	360	4

Table 6 Calculation conditions of take off

Condition	FS_{pilot}	$FS_{intermediate}$	FS_{outer}	ϕ	ϕ_P	ϕ_I	ϕ_O	T_3/K	p_4/kPa	Δ_P/%
Case 1	0.34	0.37	0.29	0.56	1.54	0.54	0.33	580	500	3.8
Case 2	0.30	0.36	0.34	0.56	1.43	0.54	0.42	580	500	3.8
Case 3	0.26	0.32	0.42	0.56	1.25	0.49	0.52	580	500	3.8
Case 4	0.19	0.36	0.45	0.56	10.84	0.52	0.52	580	500	3.8
Case 5	0.16	0.37	0.47	0.56	0.72	0.52	0.53	580	500	3.8
Case 6	0.12	0.39	0.49	0.56	0.53	0.56	0.55	580	500	3.8

2 Experimental Facility

2.1 Experimental devices

According to the test experiment of the MLDI combustion chamber of the University of Cincinnati, a cold water model experimental device of a radial stage combustion chamber with lobed nozzles is built. Figs.3,4 are the schematic diagram and physical diagram of the entire water model experimental system. The experimental devices include: A water supply system, a voltage stabilizing system, a lobed nozzle system, the experimental section and the control system. The actual length of each characteristic of the experimental platform is three times of the calculation model.

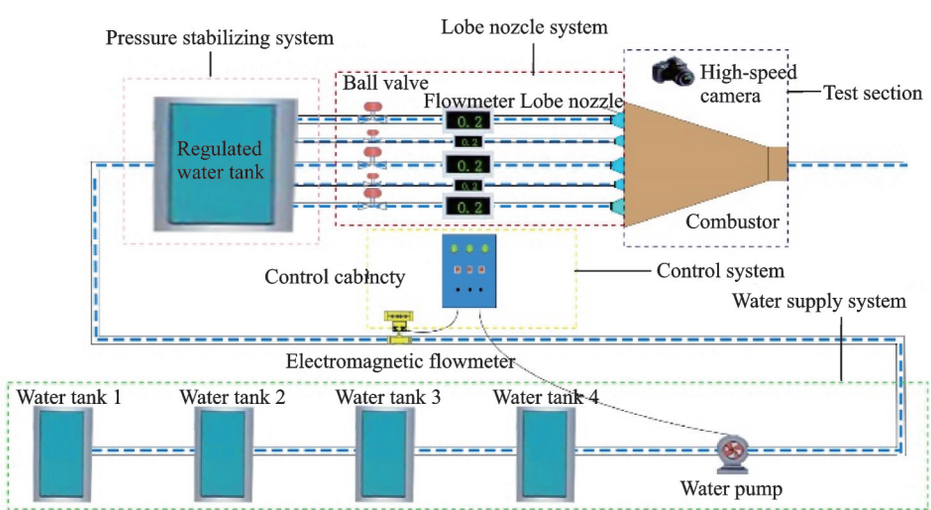

Fig.3 Schematic diagram of the experimental system

The water supply system is mainly composed of four 0.8 m^3 water tanks, water pumps and pipes. The power of the water pumps is 2.2 kW controlled by the inverter. The maximum flow rate is 65 m^3/h, and the rated flow rate is 24 m^3/h. These meet the needs of the experimental maximum flow condition. The water tanks are connected by a connector. The voltage stabilizing system is composed of a pressure stabilizing water tank, a pressure relief valve and a pressure gauge.

Since the water supply system is a single pipe, in order to stably control the water flow of different nozzles, it is necessary to use a stabilized water tank for rectification and flow control according to the working conditions. The pressure gauge is used to observe the initial pressure of water flowing into the

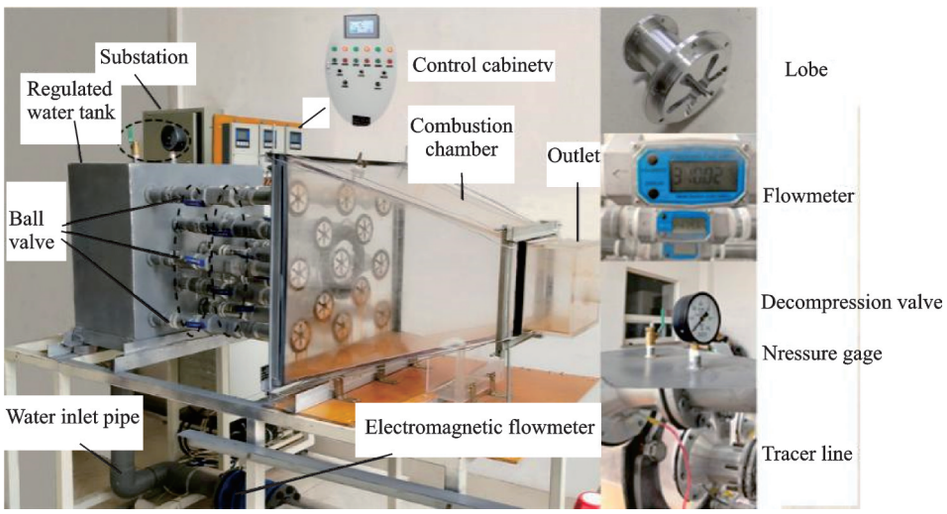

Fig.4 Experimental facility of model chamber

experimental section. The pressure relief valve is the protection system of the entire experimental device. The lobed nozzle system consists of 13 ball valves, 13 flow meters, 13 lobed nozzles and the tracer lines. Flowmeter error is $\pm 0.5\%$. The flow of each lobed nozzle line can be controlled by the ball valve and the flow meter. The experimental section consists of an inverted cone-shaped combustion chamber, a high-speed camera and a light box. The structure, size and changing shape of the vortex system in the combustion chamber can be traced and displayed by color ink and recorded with a high-speed camera. The light box provides sufficient light source for the experimental section, which is convenient for capturing the vortex structure in the combustion chamber. The control system controls the water pump and the electromagnetic flowmeter on the main pipeline, and can automatically adjust the frequency of the inverter through the program logical controller component to adjust the flow to the fixed value required by the working conditions.

2.2 Experimental program

In this paper, two working conditions in the calculation scheme are selected for the cold state verification: Partial load and take-off. In the design and development of modern aero-engine combustion chambers, it is unrealistic to carry out precise experiments on prototypes of each new-type aero-engine[20]. Modeling experiments based on the modeling theories and methods can achieve the expected results, and avoid huge expenditures, reduce the difficulty of the experiment and the experimental period, and are of great significance to the development of aviation technology[21-22]. Due to the relatively difficult visual observation of air during the experiment, and the particle image velocity technology is relatively expensive, the water flow simulation experiment method based on the dimensionless criterion number can solve the problem of difficult observation, and reduce a lot of costs and facilitate the construction of the experimental platform.

This paper uses ink as a tracer according to the Reynolds criterion in the dimensionless criterion number. In the model experiment, the water flow rate is adjusted by controling the water valve in front of the entrance of the lobe

$$Re = \frac{\rho_a \mu_a L_a}{\mu_a} = \frac{\rho_w \mu_w L_w}{\mu_w} \tag{1}$$

where the subscript "a" represents air; and "w" water. The density and dynamic viscosity of water and air are constant, and the ratio of each characteristic length of the model L_w / L_a is 3. Furthermore, the ratio of the air velocity in the simulated working condition to the water velocity in the experimental working condition can be calculated, and then converted into the water flow rate for the control of the modeling experiment. The experimental conditions of water flow modeling are shown in Tables 7—8, where FAR represents the mass ratio of fuel to air.

Table 7 Experimental conditions of partial load

Condition	ϕ	FAR	$W_f/(10^{-4}\text{kg}\cdot\text{s}^{-1})$			$W_a/(10^{-4}\text{kg}\cdot\text{s}^{-1})$			$v/(\text{m}\cdot\text{s}^{-1})$			$V/(\text{m}^3\cdot\text{h}^{-1})$
			W_{fp}	W_{fi}	W_{fo}	W_{ap}	W_{ai}	W_{ao}	v_{wp}	v_{wi}	v_{wo}	
Case 1	0.35	0.023 80	1.67	3.1	0	24.82	77.67	97.68	0.055	0.128	0.107	7.564
Case 2	0.41	0.027 88	1.67	3.1	0	21.19	66.3	83.39	0.047	0.109	0.092	6.457
Case 3	0.35	0.023 80	1.29	3.48	0	24.82	77.67	97.68	0.055	0.128	0.107	7.564
Case 4	0.41	0.027 88	1.19	3.57	0	21.19	66.3	83.39	0.047	0.109	0.092	6.457

Table 8 Experimental conditions of take off

Condition	ϕ	FAR	$W_f/(10^{-4}\text{kg}\cdot\text{s}^{-1})$			$W_a/(10^{-4}\text{kg}\cdot\text{s}^{-1})$			$v/(\text{m}\cdot\text{s}^{-1})$			$V/(\text{m}^3\cdot\text{h}^{-1})$
			W_{fp}	W_{fi}	W_{fo}	W_{ap}	W_{ai}	W_{ao}	v_{wp}	v_{wi}	v_{wo}	
Case 1	0.56	0.038 08	2.59	2.81	2.21	24.77	77.51	97.48	0.049	0.115	0.096	6.763
Case 2	0.56	0.038 08	2.28	2.74	2.59	24.77	77.51	97.48	0.049	0.115	0.096	6.763
Case 3	0.56	0.038 08	1.98	2.43	3.19	24.77	77.51	97.48	0.049	0.115	0.096	6.763
Case 4	0.56	0.038 08	1.45	2.74	3.42	24.77	77.51	97.48	0.049	0.115	0.096	6.763
Case 5	0.56	0.038 08	1.22	2.81	3.58	24.77	77.51	97.48	0.049	0.115	0.096	6.763
Case 6	0.56	0.038 08	0.91	2.97	3.73	24.77	77.51	97.48	0.049	0.115	0.096	6.763

3 Results and Discussion

3.1 Experimental results

3.1.1 Partial load (PI) experiment trace results

Fig.5 shows the results of the water flow modeling experiment of the vortex structure in the combustion chamber when the fuel distribution ratio and the total equivalence ratio (only change the amount of combustion air) are changed under the partial load conditions. ϕ displayed on the left is 0.35 and ϕ displayed on the right is 0.41; the upper row of fuel allocation is $FS_{pilot} = 0.35$, and the lower row of fuel allocation is $FS_{pilot} = 0.26$. The dotted line is perpendicular to the plane of the front end of the combustion chamber and parallel to the central axis of the combustion chamber, which is the auxiliary line for observation. At higher equivalence ratios, the inlet water flow is smaller, the size and diffusion range of the vortex system are smaller, and the mutual interference between the vortex systems occurs relatively backward, mainly in the development section. When going from a higher FS_{pilot} to a lower FS_{pilot}, at $\phi = 0.35$ (Figs.5(a,c)), the vortex structure downstream of each nozzle circuit is not much different, but the local tracer concentration has still more obvious variety. When $FS_{pilot} = 0.26$, the tracer diffusion area and local concentration of the downstream of the central pilot nozzle circuit are smaller than that when $FS_{pilot} = 0.35$, and the tracer diffusion area and local concentration of the downstream of the intermediate nozzle circuit are larger than that when $FS_{pilot} = 0.35$. In Figs. 5(b,d), due to the reduction in the amount of combustion air, the change of the tracer expansion area downstream of each nozzle circuit is much smaller, and the overall tracer diffusion area is narrower, but the changes of the local concentration of the tracer can still be observed.

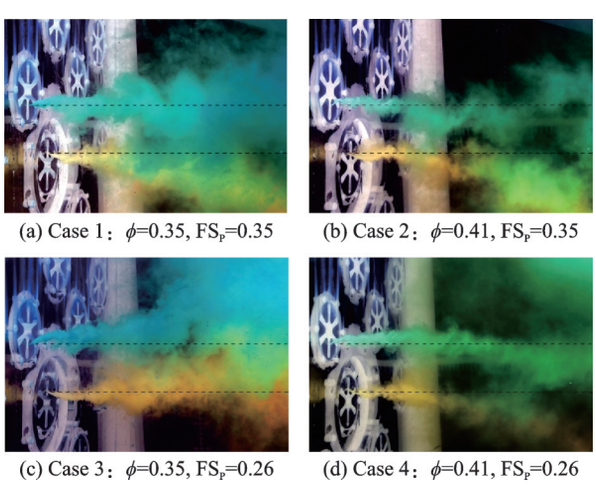

Fig.5 Trajectory tracer of the two-stage injection method experiment

3.1.2 Take off (PIO) experiment trace results

The PIO of the vortex system structure under different fuel distribution ratios is shown in Fig. 6. The total equivalence ratio remains unchanged at

0.56. The air distribution ratio remains unchanged, and only the fuel distribution ratio is changed for comparison. As the fuel distribution ratio changes, the contribution of the central pilot nozzle circuit is reduced, and the fuel flow is increased to the external nozzle circuit. A significant change in the distribution of the tracer diffusion area throughout the combustion chamber can be observed in Fig. 6(a) (FS_P=0.34, FS_I=0.37, FS_O=0.29). It shows that the tracer diffusion region downstream of each nozzle circuit is relatively independent and compact, and the downstream diffusion structure of a single nozzle circuit is relatively complete in most regions. The tracer concentration downstream of the center pilot nozzle circuit is higher in the effective distribution area. Figs. 6(a—f), the fuel distribution changes by gradually shifting the fuel flow from the central pilot circuit to the external circuit, and the intermediate circuit flow rate remains roughly unchanged. This fuel distribution method reduces the relative concentration of the local mass flow of the tracer, and the concentration distribution of the tracer in the entire flow field tends to be uniform. It can be seen from Fig. 6(f) (FS_P=0.12, FS_I=0.39, FS_O=0.49) that the tracer diffusion area downstream of the three fuel nozzle circuits is wider and the concentration distribution is more uniform compared to those in Fig. 6(a) (FS_P=0.34, FS_I=0.37, FS_O=0.29).

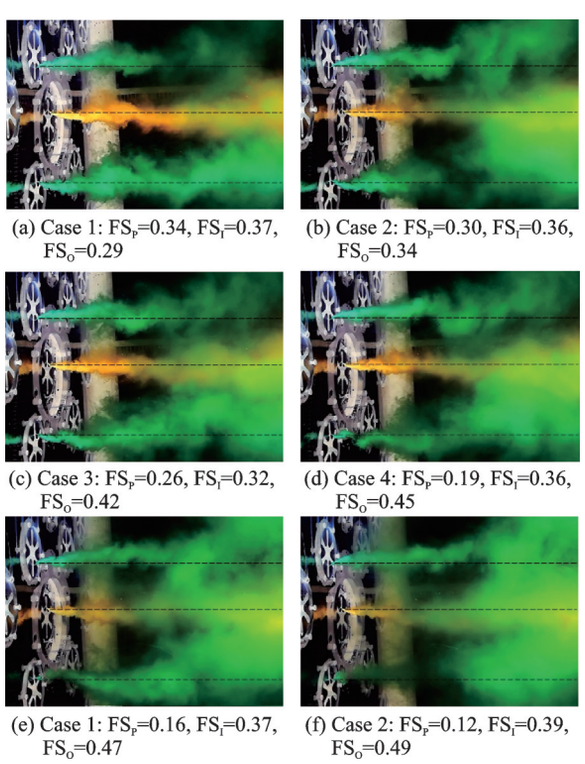

Fig. 6 Trajectory tracer of the three-stage injection method experiment

3.2 Flow field structure simulation results

Due to the special geometry of the lobed nozzle, there is a large-scale flow vortex in the downstream jet mixing flow field, which is the main reason for enhancing the flow mixing[23]. In addition, since *K-H* instability can appear in any free shear layer, there will be flow vortices and orthogonal vortices. The high intensity turbulence generated by the vortex rupture significantly improves the overall mixing process[24-25].

3.2.1 Vorticity value of flow vortex

In this paper, the orthogonal density criterion is used to define the flow vortex, and the dimensionless value of the velocity helicity is used to express the intensity of the flow vortex. Compared with other vorticity detection and evaluation standards, its main advantage is to distinguish the flow vortex in positive and negative directions. This standard can track the formation and development of complex flow vortices.

Fig. 7(a) shows the change of the vortex value along the flow direction with different equivalence ratios with the only changing of the total combustion air flow. In several working conditions under no load, due to the relatively low air flow rate, the overall change law of the vorticity values in several working conditions along the flow direction is basically similar. The vorticity value is the largest at the exit, and then drops sharply. There is a certain increase at the beginning of the transition section, and then the drop remains at a low level. However, when the air flow increases significantly, it can be clearly seen that the vorticity value changes significantly in the transition section of the combustion chamber. There are obvious differences between the two working conditions under the partial load. At ϕ = 0.35, the total air flow is relatively large, and the vorticity value of the vortex flow direction is temporarily strengthened under the interference of adjacent vortex systems. Due to the strong interac-

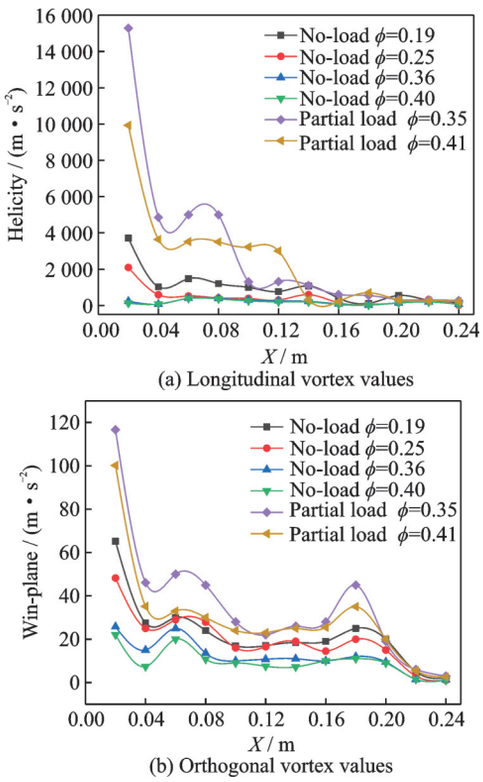

Fig.7 Vorticity varation along the flow direction under different equivalent ratios

tion between the vortex systems, the subsequent large-scale coherent structure is severely broken, and the vorticity value is quickly weakened. When $\phi = 0.41$, it is also strengthened in this section, but because the effect between adjacent vortex systems is relatively backward, there is still a certain vorticity value in the transition section. After X=0.12 m, the interaction between the vortex systems strengthens, the vortex systems begin to break up and re-construct, and the vorticity value drops rapidly.

3.2.2 Vorticity value of orthogonal vortex

Fig.7(b) shows the change of the orthogonal vorticity values along the flow direction at different equivalence ratios with the only changing of the total combustion air flow. In general, the variation law of the vorticity value of the orthogonal vortex is basically the same. The vorticity value is the largest at the outlet, and it rapidly weakens in the direction of the flow. Subsequently, due to dissipation and mutual interference between the vortex systems, the orthogonal vortex still has a certain enhancement, which is particularly evident at $X = 0.18$ m. After $X = 0.18$ m, it is already the end of the entire combustion chamber, and the vorticity value of the orthogonal vortex weakens rapidly due to the mainstream action.

3.2.3 Comparative analysis of experiment and simulation

Fig.8 shows the flow field vortex structure comparison and verification of the partial load (PI) and take-off and landing (PIO) with two-stage injection method. Fig.8 displays the combustion chamber water flow tracing experiment and the water flow simulation calculation trajectory cloud images. It can be seen that the trace result of the experimental vortex system structure and the calculation of the droplet trajectory are basically the same in its position, size and spatial extension along the experimental section. The experimental observations of streamlines and the calculation results are in agreement, which proves that the numerical calculation is correct and credible. This provides a reliable modeling basis for the future use of water simulation experiments to study the aerodynamic characteristics of the flow field in the aeroengine combustion chamber and the organization of combustion.

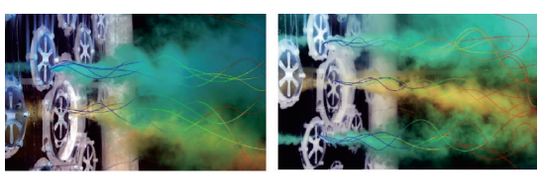

Fig.8 Comparison between the experimental and numerical simulation results

3.3 Comparison of combustion OH* distribution

For the combustion mechanism of fuel oil, OH* is an oxidized radical produced by the fuel combustion reaction, so it is generally believed that the OH* concentration distribution can represent the combustion flame field. Therefore, OH* concentration can be used as the basis for comparative analysis of actual measurement and calculation of combustion flames. The University of Cincinnati used the OH* chemiluminescence method in the actual measurement of the combustion flame of the swirl combustor. In this paper, the OH* concentration distri-

bution of the lobe combustor calculated by combustion is compared with the experimental results of the swirl combustor[1]. The realizable k-e turbulence model is selected in the calculation process, and the standard wall function method is adopted to treat the wall surface. The Euler-Lagrange method is used as the discrete phase model. The fuel spray model is used for the conical nozzle model. Non-premixed combustion model is adopted and its radiation model is simulated with the DO method. Velocity inlet, pressure outlet and wall surface mixed wall surface are used for various boundary conditions.

3.3.1 No-load (P)

Fig.9 is a comparison chart of the measured results of the hydroxyl group of the swirl combustion chamber and the calculation result of the OH* combustion of the lobe combustion chamber under different equivalent ratios when only the pilot exhaust nozzle is used. It can be seen that fuel is ignited and burned after being injected into the combustion chamber. As the equivalence ratio increases, the flame range becomes wider in the radial direction and longer in the axial direction. The local combustion temperature becomes lower and the flame core area gradually expands. Comparing the measured OH* of the flame experiment of the swirl combustor with the calculation result of the flame OH* of the combustion mechanism of the lobe combustor, we find that at low equivalence ratio (Fig.9(a)), the combustion flame of the swirl combustor experiment is fan-shaped. As the equivalence ratio increases, the fan-shaped surface becomes narrower (Fig.9(d)). The OH* concentration calculated by the combustion mechanism of the lobe combustor is mushroom-shaped when the equivalence ratio is low (Figs.9(a,b)). With the increase of the equivalence ratio, the mushroom shape gradually becomes ellipsoidal (Fig.9(c,d)). Due to the difference in the combustion organization of the lobe combustion chamber and the swirl combustion chamber, the shape of the combustion flame should be different under the same working conditions.

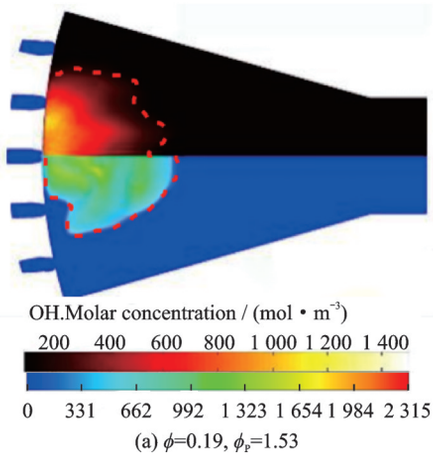

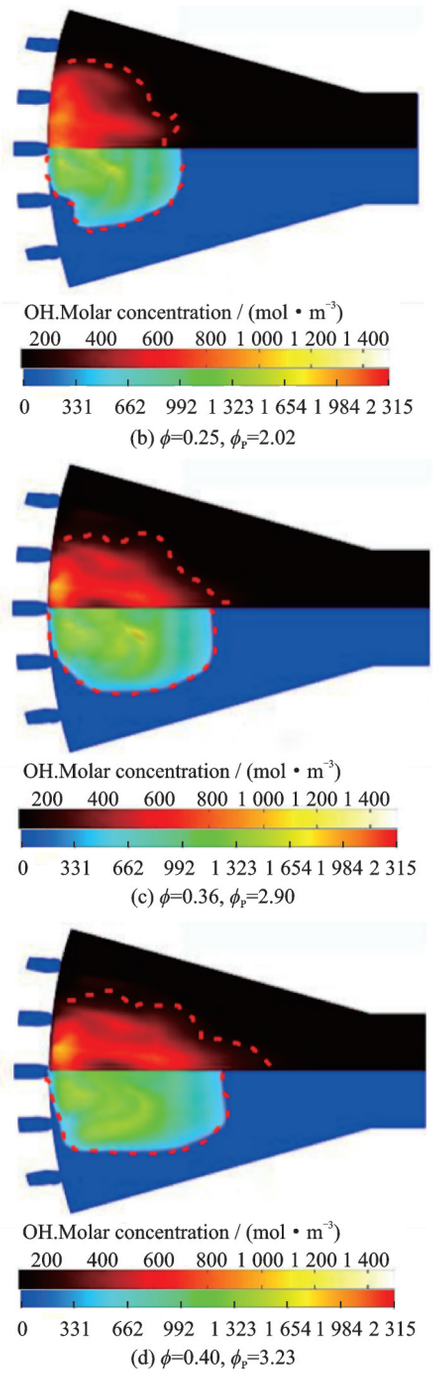

Fig.9 Pilot only v.s. ϕ with T_3=496 K, p_4=100 kPa, and Δ_P=4.1%

3.3.2 Partial load (PI)

When the center pilot row nozzle and the intermediate row nozzle use different fuel distribution ratios and different total equivalence ratios, the measured results of the OH* flame chemiluminescence of the swirl combustion chamber, and the calculated OH* concentration results of the lobe combustion chamber are shown in Fig.10. At higher equivalence ratios, the heat release area becomes significantly larger. Under different fuel distribution ratios, when going from a higher FS_{pilot} to a lower FS_{pilot}, at $\phi = 0.35$, Figs.10(a, c) show the reaction zone downstream of the central pilot nozzle loop and the intermediate nozzle circuit, and the heat release intensity changes significantly. The heat release intensity of the reaction zone downstream of the center pilot nozzle circuit is reduced. The heat release region of the reaction zone downstream of the intermediate nozzle circuit becomes longer, and the flame distribution is more uniform. Comparing the measured results of the swirling flame with the calculation results of the lobe flame, we find that the changes are basically the same, but the shape of the flame is somewhat different.

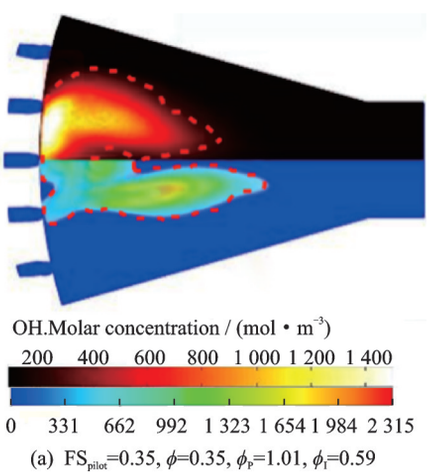

(a) FS_{pilot}=0.35, ϕ=0.35, ϕ_P=1.01, ϕ_I=0.59

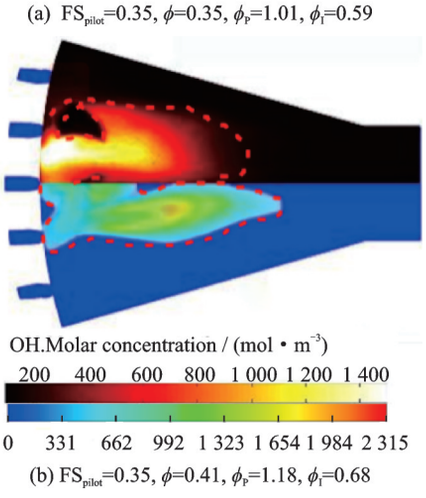

(b) FS_{pilot}=0.35, ϕ=0.41, ϕ_P=1.18, ϕ_I=0.68

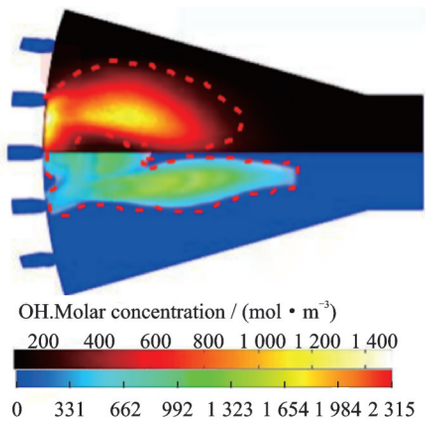

(c) FS_{pilot}=0.27, ϕ=0.35, ϕ_P=0.78, ϕ_I=0.59

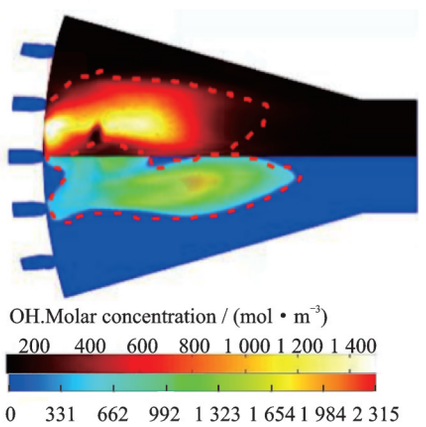

(d) FS_{pilot}=0.25, ϕ=0.41, ϕ_P=0.82, ϕ_I=0.79

Fig.10 Pilot and intermediate fuel circuits with varying ϕ and T_3=496 K, p_4=360 kPa, Δ_P=4.0%

3.3.3 Partial load (PIO)

Fig.11 shows the measured results of the OH* flame in the swirl combustion chamber and the calculated OH* concentration of the lobe combustion chamber under different fuel distribution ratios (PIO). It can be seen that the measured trend of the swirling flame and the calculation result of the lobe flame are basically the same, but there are differences in the organization, which leads to a significant difference in the flame shape. By changing the fuel distribution method, reducing the fuel contribution from the central pilot nozzle circuit and increasing the fuel flow to the external nozzle circuit, the distribution of OH* intensity levels has a large change. In Fig.11(a), due to the higher local equivalent, the local heat release intensity of OH* is higher, and the central pilot and intermediate fuel circuit dominate. The heat release area of the external nozzle cir-

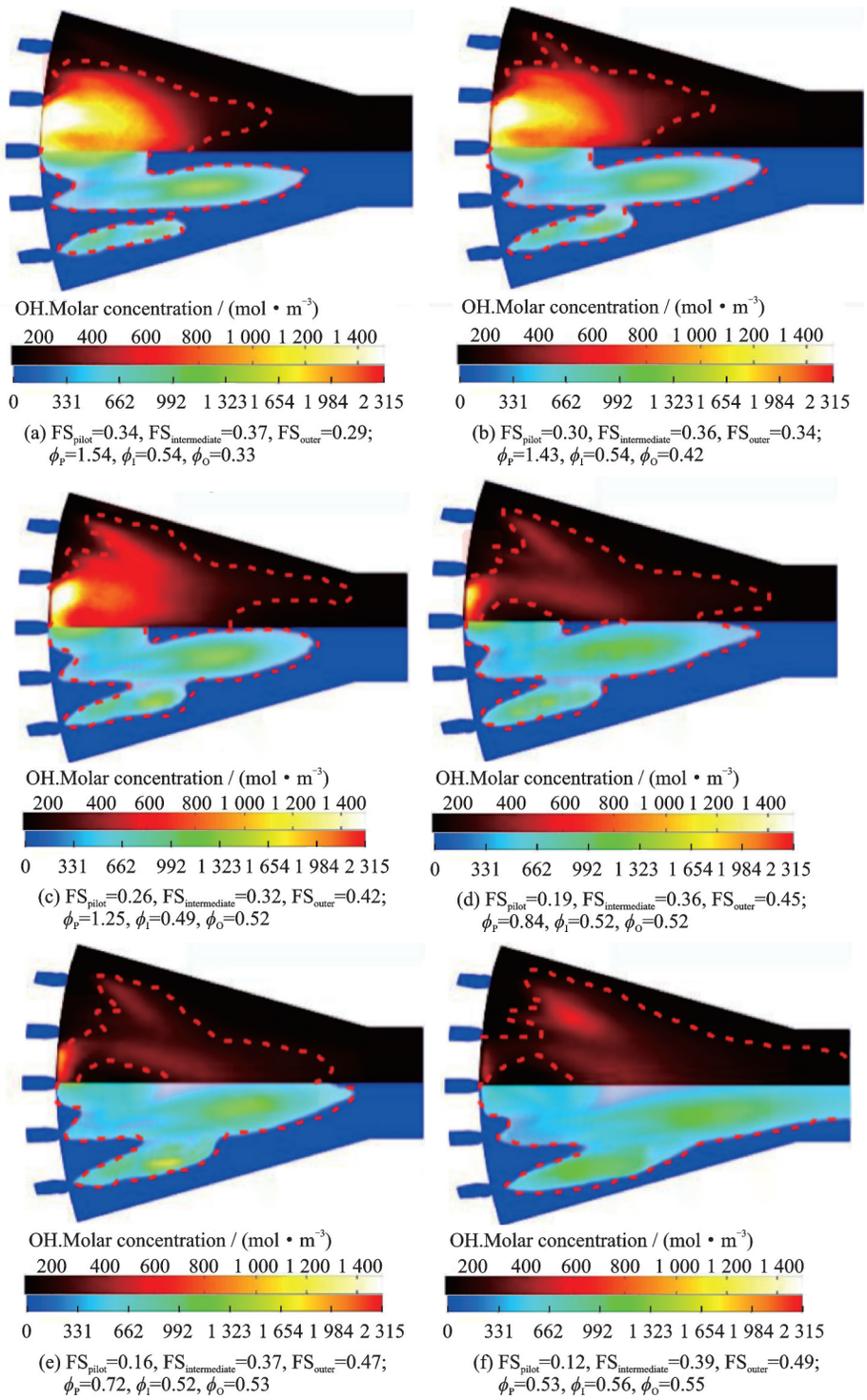

Fig.11 All fuel circuits with varying fuel split with T_3=580 K, p_4=500 kPa, ϕ=0.56, Δ_P=3.8%

cuit is weak and limited in scope. In Figs.11(a—f), the fuel distribution is changed by transferring the fuel flow of the central pilot circuit to the external nozzle circuit, and the flow rate of the intermediate nozzle circuit remains basically unchanged. This distribution method makes the fuel distribution more uniform, and the local equivalent ratio is more even. The OH* luminous intensity of the swirling combustion chamber and the OH* concentration distribution of the lobe combustion chamber are more uniform. In Fig.11(f), the local equivalent ratios of the three fuel circuit reaction zones are very close to the total equivalent ratio of the combustion chamber. Even if there is a small but relatively bright heat release zone in the downstream reaction zone of the central pilot circuit in Fig.11(e). The intensity in

Fig. 11(f) is significantly reduced, which is similar to the intensity of other reaction zones in the combustion chamber. Such performance fully demonstrates the uniform fuel distribution fact.

3.4 Combustion performance analysis

3.4.1 Outlet temperature distribution factor

The outlet temperature distribution factor (OTDF) is an important parameter for evaluating the quality of the temperature field at the outlet of the combustion chamber. The smaller the OTDF value is, the better the quality of the outlet temperature field is, the longer the service life of the turbine blade is, and the higher the reliability of the work is. In general, the OTDF index should be controlled below 0.35, and is defined as

$$\mathrm{OTDF}=\frac{T_{4\max}-\bar{T}_4}{\bar{T}_4-T_3} \tag{2}$$

where T_{4max} is the maximum temperature of the combustion chamber outlet; T_4 the average temperature of the combustion chamber outlet; and T_3 the average temperature of the combustion chamber inlet. The OTDF values for each calculation condition are shown in Fig. 12. Under no-load conditions, OTDF increases with the increase of the equivalence ratio. When the equivalence ratio increases at the partial load, OTDF also becomes larger (Case 1 and Case 3, Case 2 and Case 4), and when the fuel flow rate of the central pilot circuit is reduced, OTDF also becomes smaller (Case 1 and Case 2, Case 3 and Case 4). Under cruise conditions, when the PI injection method is used, the OTDF value is large, and the quality of the outlet temperature field is relatively poor. When the PIO injection method is used, the OTDF value is significantly reduced. The PIO injection method is used for take-off conditions. As the fuel flow from the central pilot circuit is transferred to the external nozzle circuit, the OTDF value gradually decreases. Overall, when the PIO fuel injection method is used, the vortex structure induced downstream of each nozzle circuit can be fully utilized, and the oil-gas blending effect is better and the combustion is uniform. Therefore, OTDF is smaller and the quality of the exit temperature field is better. Diverting the fuel flow from the central pilot circuit to the external nozzle circuit can also improve the quality of the outlet temperature field. In addition, as the equivalence ratio increases, the OTDF value becomes larger and the quality of the outlet temperature field becomes worse.

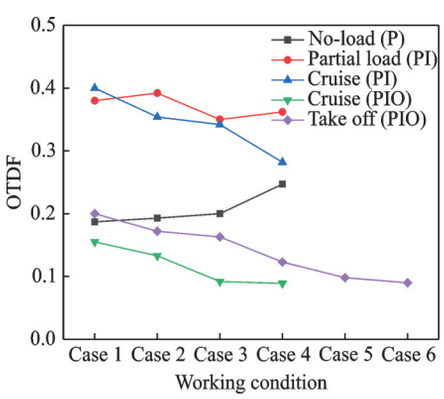

Fig.12 Outlet temperature distribution factor

3.4.2 Emission analysis

The pollutant emission index is generally expressed by EI, which can reflect the degree of conversion of chemical energy and thermal energy during the combustion process. The viation kerosene used in this article has a low N content, so fuel-based NO_X is not considered. EI is defined as

$$\mathrm{EI}=g_{\mathrm{pollution}}/kg_{\mathrm{fuel}} \tag{3}$$

Fig. 13 shows the comparison between the calculated NO_X emissions of the lobe combustion chamber and the experimental NO_X emissions of the swirl combustion chamber for each operating condition. Under different operating conditions, the NO_X emissions of the lobe combustion chamber and the swirl combustion chamber are basically the same. The overall NO_X emissions of the lobe combustion chamber are slightly higher than the experimental values of the swirl combustion chamber. Under no-load conditions, the simulation calculation results are close to the experimental results. As the equivalence ratio increases, emissions also increase. Under this condition, the local equivalent is relatively high, the fuel combustion is incomplete, the combustion temperature is low, and the NO_X emissions are also relatively low. When the equivalence ratio increases at the partial load, the NO_X emissions become larger (Case 1 and Case 2, Case 3 and Case 4), and when the fuel flow of the central pilot circuit is reduced, the NO_X emissions become smaller (Case 1 and

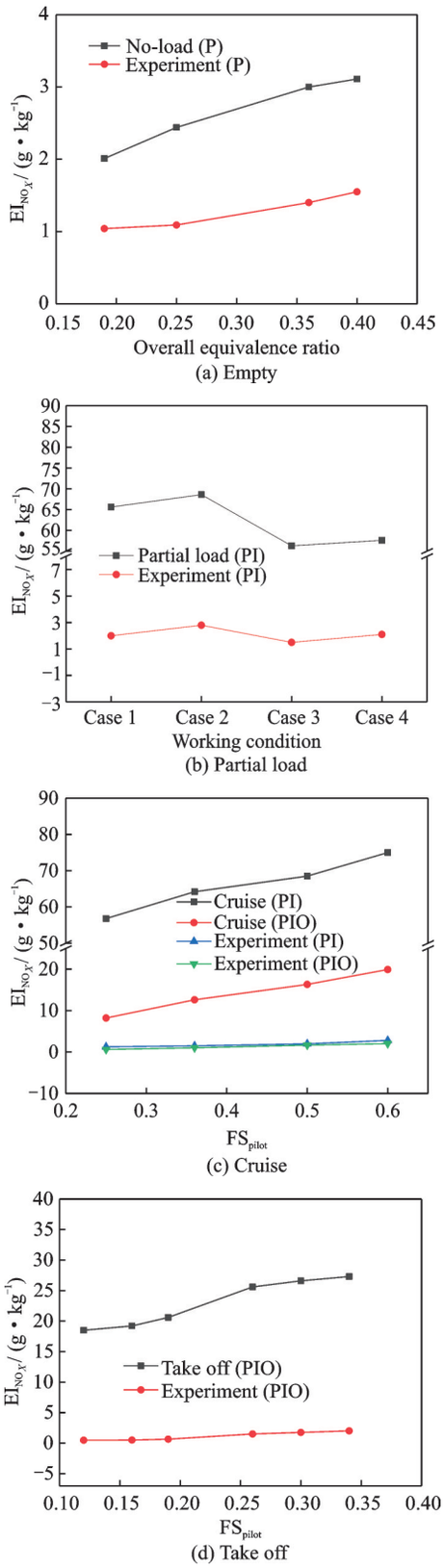

Fig.13 NO_X emission of different working conditions

Case 3, Case 2 and Case 4). This is mainly because when the fuel flow of the central pilot circuit is transferred to the external nozzle circuit, the local equivalence ratio becomes smaller, the local high temperature decreases, and the generated thermal NO_X naturally becomes smaller. Under cruise conditions, different fuel injection methods have a great influence on NO_X emissions. The PIO injection method produces significantly less NO_X than the PI injection method, and the NO_X emissions increase when the fuel flow from the external circuit is transferred to the pilot nozzle. Since the take-off condition is a three-stage fuel injection method, the overall NO_X emissions are low, and the NO_X emissions also increase when the external circuit fuel flow is transferred to the pilot circuit. The above analysis shows that the local equivalence ratio plays a vital role in NO_X emissions. When the PIO fuel injection method is used, the local equivalent downstream of each nozzle circuit is relatively low, the vortex structure induced by the lobed nozzle can maximize participation in the oil and gas blending process, and the NO_X emissions are also low. When the external circuit fuel flow is transferred to the central pilot circuit, the local equivalent ratio downstream of the central pilot circuit increases, and the magnitude of the local equivalent ratio downstream of each circuit is inconsistent. This will cause local high temperature, uneven combustion, and increased NO_X emissions.

3.4.3 Combustion efficiency

Combustion efficiency is an important parameter for evaluating the completeness of fuel combustion. There are many influencing factors, such as the geometry of the combustion chamber, the chemical reaction process, etc. The combustion efficiency is defined as

$$\eta = 1 - \left[\frac{EI_{CO}LHV_{CO} + EI_{CH_4}LHV_{CH_4}}{1\,000LHV}\right] \times 100\% \tag{4}$$

where EI is the pollutant emission index; and LHV the low heating value of the fuel. The results of combustion efficiency calculations for various operating conditions are shown in Fig.14. The combustion efficiency is overall above 98%. Among them, when the equivalence ratio increases under no-load conditions, the vorticity values of the flow vortex and orthogonal vortex in the combustion chamber decrease, the local equivalent is relatively high, and the combustion efficiency decreases gradually below

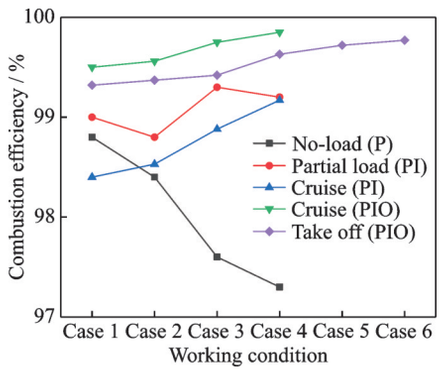

Fig.14 Combustion efficiency of different conditions

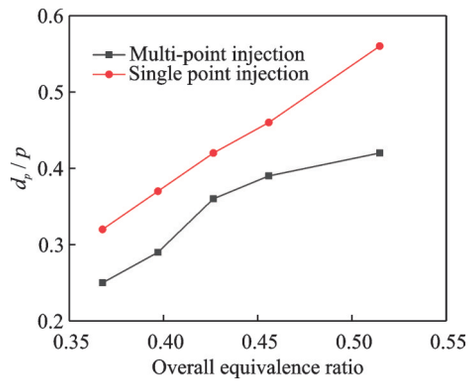

Fig.15 Total pressure recovery coefficients of different injection modes

98%. When the equivalence ratio increases at the partial load, the combustion efficiency also becomes smaller (Case 1 and Case 2, Case 3 and Case 4). When the fuel distribution ratio changes and the fuel flow of the center pilot nozzle circuit is transferred to the middle nozzle circuit, due to the reduction of the local equivalence ratio of the reaction zone downstream of the center pilot nozzle circuit, the fuel combustion is relatively sufficient and the combustion efficiency becomes larger (Case 1 and Case 3, Case 2 and Case 4). Under cruise conditions, the combustion efficiency is lower when PI fuel injection is used. When the PIO fuel injection method is adopted, the combustion efficiency is significantly increased. Both fuel injection methods increase the combustion efficiency as the fuel flow from the central pilot nozzle circuit is transferred to the external nozzle circuit. This is because the fuel distribution method changes, the distribution ratio of fuel to combustion air tends to be uniform, and the local equivalent is relatively low. The take-off conditions further confirm the changing characteristics of combustion efficiency during the cruise PIO injection mode.

3.4.4 Total pressure recovery coefficient

The total pressure recovery coefficient refers to the ratio of the total outlet pressure of the combustion chamber to the total inlet pressure. It is an index used to characterize the loss of pressure potential energy when gas flows through the combustion chamber. The lower the total pressure recovery coefficient is, the greater the total pressure and power loss is, and the higher the fuel consumption rate is. Fig.15 is a comparison result of the total pressure recovery coefficient of a multi-point lobed nozzle radial stage combustion chamber and a single large-lobed nozzle combustion chamber where d_p/p is the total pressure recovery coefficient. It can be seen that because the vortex system downstream of the multi-point lobe combustion chamber is more abundant than the single-point lobe combustion chamber, the interaction between the vortex systems is stronger, and the flow mixing brings additional total pressure loss. Therefore, the total pressure recovery coefficient of the multi-point lobe combustion chamber is generally smaller than that of the traditional single large-lobe combustion chamber, and the total pressure loss is greater. The total pressure recovery coefficient gradually increases as the equivalence ratio increases. This is related to the reduction of the dimensionless value of the vortex system structure at the high equivalence ratio as the total pressure recovery coefficient increases and the total pressure loss decreases.

4 Conclusions

The water model experiments demonstrate that the vortex structure is induced by the radial cascade combustion chamber as the lobed nozzles form the initial section, transition section and development section. The vortex system downstream of each nozzle circuit in the initial stage is relatively independent and complete. The vortex structure of the transition section expands in scope while spiraling forward. The interaction between adjacent vortex systems in the development section makes the reorganized large-scale coherent structure that fills most of the space of the combustion chamber. The three-

stage PIO injection method has a more uniform flow field distribution than the two-stage PI injection method. It can be seen from the numerical results of the cold state that the vorticity values of the flow vortex and the orthogonal vortex are similar along the flow direction. The vorticity value is the largest at the exit of the lobed nozzles, and then drops sharply. As X ranges between 0.06—0.08 m, the vorticity value starts to increase slightly due to mutual interference during the vortex systems. Subsequently, due to the interference enhancement and dissipation effects, the single complete vortex system structure is broken. In addition, the vortex value of the flow vortex is weakened and remains at a low level. The orthogonal vortex still has a certain amount of vorticity in the development stage due to the interaction between the vortex systems, and then is quickly weakened due to the mainstream effect. When the total equivalence ratio increases with only the amount of combustion air increasing, the vortex values of the flow vortex and orthogonal vortex decrease at various positions along the flow direction. The agreement between the water flow modeling experiment and the numerical research results verifies the feasibility of the modeling method and the credibility of the modeling results, although the similarity theory has certain limitations.

The comparison between the calculation results of the OH* concentration distribution of the radial cascade combustion chamber with the lobed nozzles and the OH* luminescence experiment results of the swirl nozzle array combustion chamber demonstrates that the change law of the combustion field along the flow direction with each influencing factor is basically the same, but the different organization methods lead to differences in the shape of the combustion field. As the equivalence ratio increases, the distribution range of the combustion field increases. When the fuel flow of the central pilot nozzle circuit is gradually transferred to the external nozzle circuit, the flame distribution of the entire combustion field is more uniform.

The following conclusions are drawn from the performance analysis of the radial cascade combustion chamber with lobed nozzles: When the total equivalence ratio increases, OTDF of the combustion chamber increases, the quality of the outlet temperature field deteriorates, the NO_X emissions increase, and the combustion efficiency becomes lower. For the three-stage fuel injection mode (PIO), the temperature field distribution of the combustion chamber is more uniform than that of the two-stage fuel injection mode (PI), the local equivalent ratio is smaller, the outlet temperature field quality is better, the NO_X emissions are smaller, and the combustion efficiency is higher. When the fuel distribution method is changed and the fuel flow of the central pilot nozzle circuit is gradually transferred to the external nozzle circuit, the quality of the temperature field at the outlet of the combustion chamber becomes better, the NO_X emission decreases, and the combustion efficiency increases. Even if the total equivalence ratio is large, when the fuel distribution method is changed, the local equivalence ratio will be greatly reduced, and the various indices of the combustion chamber will also tend to be favorable.

References

[1] VILLALVA R, DOLAN B J, MUNDAY D, et al. Experimental study of a multinozzle combustor at elevated pressures[J]. AIAA Journal, 2015, 53(4): 986-1001.

[2] ACOSTA W A, CHANG C T. Comparison of combustion dynamic characteristics of two advanced multicup fuel injectors[C]//Proceedings of the 2018 Joint Propulsion Conference. Cincinnati, USA: AIAA, 2018: 4559.

[3] HE Z, CHANG C. Combustion dynamic characteristics identification in a 9-point LDI combustor under choked outlet boundary conditions[C]//Proceedings of the 55th AIAA Aerospace Sciences Meeting. Grapevine, USA: AIAA, 2017: 0779.

[4] DICKSON N. Local air quality and ICAO engine emissions standards[R]. USA: ICAO Air Transport Bureau, 2014.

[5] AHMED A, HASEMAN J, TAMBE S, et al. Experimental study of a low-NO_X lean direct injection combustor design[C]//Proceedings of ASME Turbo Expo 2016: Turbo Machinery Technical Conference and Exposition. Seoul, South Korea: ASME, 2016, 49750: V04AT04A027.

[6] HICKS Y R, TEDDER S A, ANDERSON R. Alter-

native bio-derived JP-8 class fuel and JP-8 fuel: Flame tube combustor test results compared using a GE taps injector configuration[C]//Proceedings of the 52nd AIAA/SAE/ASEE Joint Propulsion Conference. Salt Lake City, USA: AIAA, 2016: 4890.

[7] SURGENOR A. A path to N+3 fuel-flexible combustors: GRC-E-DAA-TN30828 [R]. USA: NTRS, 2016.

[8] VILLAVA R, DOLAN B, MUNDAY D, et al. Medium pressure emissions of a multipoint low NO_X combustion system[C]//Proceedings of the 51st AIAA Aerospace Sciences Meeting Including the New Horizons Forum and Aerospace Exposition. Grapevine, USA: AIAA, 2013: 1044.

[9] LI S, ZHANG S, ZHOU H, et al. Analysis of air-staged combustion of NH_3/CH_4 mixture with low NO_X emission at gas turbine conditions in model combustors[J]. Fuel, 2019, 237: 50-59.

[10] YOLANDA R H, TYLER C, ROBERT A. Flame tube testing of a GEA TAPS injector: Effects of fuel staging on combustor fuel spray patterns, flow structure, and speciation[C]//Proceedings of the 2018 Joint Propulsion Conference. Cincinnati, USA: NASA, 2018: 4476.

[11] LEE C M, TACINA K M, WEY C. High pressure low NO_X emissions research: Recent progress at NASA Glenn Research Center[EB/OL]. (2007-01-01).https://ntrs.nasa.gov/citations/20070022362.

[12] TACINA R, MAO C P, WEY C. Experimental investigation of a multiplex fuel injector module with discrete jet swirlers for low emission combustors[C]//Proceedings of the 42nd Aerospace Sciences Meeting and Exhibit. Reno, USA: AIAA, 2004.

[13] PROCIW A, RYON J, GOEKE J. Low NO_X combustion concepts in support of the NASA environmentally responsible aircraft program[C]//Proceedings of ASME Turbo Expo 2012. Copenhagen, Sweden: ASME, 2012.

[14] HICKS Y, ANDERSON R, LOCKE R. Optical measurements in a combustor using a 9-point swirl-venturi fuel injector[C]//Proceedings of the 18th International Symposium on Air Breathing Engines. Beijing, China: [s.n.], 2007.

[15] MARTIN C, GROETZ R, YOO J, et al. Demonstration of swirl-controlled 3D-printed mesoscale burner array using gaseous hydrocarbon fuels[C]//Proceedings of the 55th AIAA Aerospace Sciences Meeting. Grapevine, USA: AIAA, 2017: 1778.

[16] LI G, ZHAO Y J, LIU C X, et al. The design and characteristics of a novel injector: A lobed swirl injector[C]//Proceedings of Turbo Expo: Power for Land, Sea, and Air. American Society of Mechanical Engineers. Charlotte, USA: ASME, 2017: 50848.

[17] LI G, XI J, ZHU J, et al. Combustion control using a lobed swirl injector and a plasma swirler[J]. Applied Thermal Engineering, 2019, 152: 92-102.

[18] GEHRKE A, WUENSCH O, RUETTEN M. Integral surface analysis of vortical lobed nozzle flows[C]//Proceedings of the 55th AIAA Aerospace Sciences Meeting. Texas, USA:AIAA,2017: 1706.

[19] XIE Y, ZHONG C, YUAN D F, et al. Combustion characteristics of micro-lobed burners[J]. Journal of Northeastern (Natural Science), 2017(4): 536-541.

[20] PRESZ W, GREITZER E. A useful similarity principle for jet engine exhaust system performance[C]//Proceedings of the 24th Joint Propulsion Conference. Boston, USA: [s.n.], 1988: 3001.

[21] XIA C J, WANG D. Improved correction methods of aircraft engine fan speed based on similarity theory[J]. Journal of Aerospace Power, 2016, 31(4): 941-947.

[22] ZHAO Q X. Application of similitude principle in the development of combustion chamber[J]. Aviation Maintenance & Engineering, 1997(2): 4-7.

[23] PATERSON R W. Turbofan mixer nozzle flow field: A benchmark experimental study[J]. ASME Gas Turbines Power, 1984, 106(3): 692-698.

[24] RICHARDS C D, SAMUELSEN G S. The role of primary jets in the dome region aerodynamics of a model can combustor[C]//Proceedings of ASME 1990 International Gas Turbine and Aeroengine Congress and Exposition. Belgium: ASME, 1990.

[25] ELLIOTT J, MANNING T, QIU Y, et al. Computational and experimental studies of flow in multi-lobed forcedmixers[C]//Proceedings of the 28th Joint Propulsion Conference and Exhibit. Nashville, USA: AIAA, 1992: 3568.

Acknowledgements This work was supported by the Liaoning Provincial Natural Science Joint Fund Project (No. 120316013). The authors would like to acknowledge the following people for their assistance: DU Xiaocheng, WU Zhonggang and all the staff at the Key Laboratory of Energy and Environment, Shenyang Aerospace University.

Author Dr. **WANG Lijun** received his Ph.D. degree of thermal energy and power engineering in 2004. Now he is an associate professor of Shenyang Aerospace University. His research focuses on aviation engine combustion chamber design and

analysis, engineering thermal physics and other researches.

Author contributions Dr. **WANG Lijun** designed the study, complied the models, conducted the CFD simulation, experiments and analysis, and revised the manuscript data and wrote the manuscript. Mr. **FAN Jingpeng** contributed to the simulation and experiment data and revised the manuscript. Mr. **MEN Kuo** and Mr. **XU Yijun** participated in experimental sample collection and figure generation. All authors commented on the manuscript draft and approved the submission.

Competing interests The authors declare no competing interests.

(Production Editor: ZHANG Bei)

波瓣喷嘴径向分级燃烧室的燃烧性能研究

王力军，范荆鹏，门 阔，徐义俊

(沈阳航空航天大学能源与环境学院，沈阳 110136，中国)

摘要：为了探究波瓣喷嘴径向分级方式对流场组织方式的影响，搭建了13点波瓣喷嘴径向分级燃烧室冷态水模实验台。对比辛辛那提大学测试的一系列燃烧羟基发光实验，选取空载、部分载荷、巡航和起飞4种对应的工况，对当量比、燃料喷射方式和燃料喷射比例等因素下波瓣喷嘴径向分级燃烧室内的流场涡系结构、涡量值、燃烧多物量场以及燃烧特性，进行了数值研究。结果表明：在不同影响因素下，波瓣燃烧室的羟基火焰场变化规律与旋流燃烧室羟基发光实验变化规律基本相同，但其火焰场形状存在较大差别。局部当量比对燃烧室的相关燃烧性能影响较大。较低当量比、3级空气和燃料喷射方式以及将先导回路燃料流逐渐转移到外部回路的条件下，燃烧室的温场、火焰场分布比较均匀，出口温度场品质较好，燃烧效率较高，NO_x排放量比较低，与冷态实验结果基本符合。冷态实验结果说明了流场组织方式对燃烧组织方式影响的重要性，同时也验证了计算结果的可靠性。

关键词：波瓣喷嘴；径向分级燃烧室；气动特性；燃烧特性